Joint Stick-Slip Friction Compensation of Robot Manipulators by Using Smooth Robust Controllers

L. Cai* and G. Song†
Department of Mechanical Engineering
Columbia University
New York, NY 10027

Received June 25, 1993; revised September 2, 1993
Accepted October 1, 1993

In this article, two new smooth robust nonlinear compensators have been developed, respectively, for positional regulation and trajectory tracking of rigid robot manipulators with internal joint stick-slip friction. The proposed controllers can improve not only the positioning accuracy but also the smoothness of motion. No exact knowledge of the friction models is required for the design of the controllers. Furthermore, the tracking controller is also robust with respect to the uncertain link parameters. Using Lyapunov's direct method, we can show that the time-invariant positional regulation controller guarantees the global boundedness stability of the closed-loop system, while the time-varying positional tracking controller guarantees the global asymptotic stability of the closed-loop system. The numerical simulations of the controllers on a two-link robot are presented as illustrations.

この発表では、内部にジョイントの吸着滑り摩擦が発生するリジッド・ロボット・マニピュレータの位置制御とトラッキングを改善するために開発した、2つの新しいスムースで強力な非線形補償器について説明する。今回提案するコントローラは、位置精度だけではなく、動作の円滑さについても改善されている。このコントローラの設計では、摩擦モデルの正確な知識は要求されない。リヤノフの直接法を使い、時間変動型の位置トラキング・コントローラが閉ループ・システムの全領域においては漸近的な安定性しか保証できないのに対して、時間不変型の位置制御コントローラは閉ループ・システムの全領域において安定であることを示す。数学的シミュレーションは、2リンク・ロボットについて行う。

*Now with the Department of Mechanical Engineering, Hong Kong University of Science and Technology, Kowloon, Hong Kong.
†To whom all correspondence should be addressed.

Journal of Robotic Systems 11(6), 451–470 (1994)

CCC 0741-2223/94/060451-020

1. INTRODUCTION

As natural resistance when relative motion or the tendency of motion is involved, stick-slip friction, also called dry friction, exists in almost all mechanisms. Positioning inaccuracy and motion intermittency in servo-mechanisms often result from the existence of stick-slip friction. Mechanical methods have been used to attenuate the effect of stick-slip friction, but this nonlinear phenomenon still exists to some degree. Stick-slip friction modeling and compensation receive considerable attention in robotic applications.[1-7] A recent study of the detrimental effect of friction on space microgravity robotics reveals that the smoothness of motion becomes an important issue because the dynamic interaction between the regular control force and Coulomb friction results in harmful acceleration disturbances.[5] Thus the controller is required to achieve not only high accuracy but also smooth motion.

A wide range of friction compensation techniques has been proposed. The traditional PD controller will not achieve satisfactory results because of the steady-state error. Even though the error may be reduced by increasing the proportional gain, the high-gain controller brings drawbacks, such as causing system instability when the drive train is compliant or leading to saturation. PID controllers will provoke the generation of limit cycles[8,9] and thus are not suitable for stick-slip friction compensation.

Many researchers have pointed out that attempts to linearize the friction model may lead to incorrect predictions of the system behavior,[10,11] for instance, linearization fails to predict limit cycles. Friction forward cancellation technique only works well when the friction model is known exactly. Adaptive friction compensation schemes have been proposed to compensate nonlinear friction in a variety of mechanisms,[12-15] but these are usually based on the linearized model or the model with linearized parameters. Each model is an approximation of the actual nonlinear system.

Robust controllers have been developed to strengthen the compensation of the nonlinear friction. Canudas et al.[3] designed a linear compensator robustifying the closed-loop system under the eventuality of the inexact friction compensation induced by adaptive transients and other external disturbances.[16] Southward et al.[10] implemented a robust nonlinear proportional feedback controller to compensate for stick-slip friction for a single degree-of-freedom (dof) object and achieved asymptotic stability. However, it appears to be a bang-bang force in a region near the desired reference and thus causes extra acceleration disturbances. The current existing controllers, which can improve the accuracy of steady-state positioning under the influence of dry friction, do not increase the smoothness of motion and sometimes even cause the system to experience more acceleration disturbances.

In this article, two novel smooth robust nonlinear controllers, one for positional regulation and one for trajectory tracking, are proposed for rigid robot manipulators with internal joint friction. The proposed controllers have the advantages of avoiding chattering and ensuring smooth motion. Both controllers consist of three parts: feedforward term(s), linear feedback term(s), and a nonlinear smooth robust compensator. With prior knowledge of the maximum static friction torque at each joint, the time-invariant controller for positional regulation guarantees global boundedness stability of the closed-loop system. On the other hand, with prior knowledge of the upper bounds of maximum static friction torques and uncertain link parameters as well as the upper bounding functions of slipping torques, the time-varying tracking controller guarantees global asymptotic stability of the closed-loop system.

Lyapunov's second method has been used to prove the global stability of the closed-loop systems. When the proposed regulator is applied, the steady-state error can be adjusted to any small value by the parameters of the controller on consideration of both the required accuracy and the available resolution of the sensor, whereas the desired transient can be achieved by adjusting the controller parameters when the tracking controller is implemented. The proposed positional regulator and trajectory tracking controller are successfully tested on a two dof manipulator by numerical simulations.

2. SYSTEM DESCRIPTION AND MODELING

2.1. Friction Modeling

Stick-slip friction is present in any elements involving relative motion in robot mechanisms such as gears, pulleys, bearings, DC motors, and so forth. Stick-slip friction is generally described as a composite of two different processes: the static process when an object is stationary and is likely to move under certain applied torque, and the dynamic process when motion is involved. The static process is characterized by the maximum static torque (or breakaway torque), under which the static state remains.

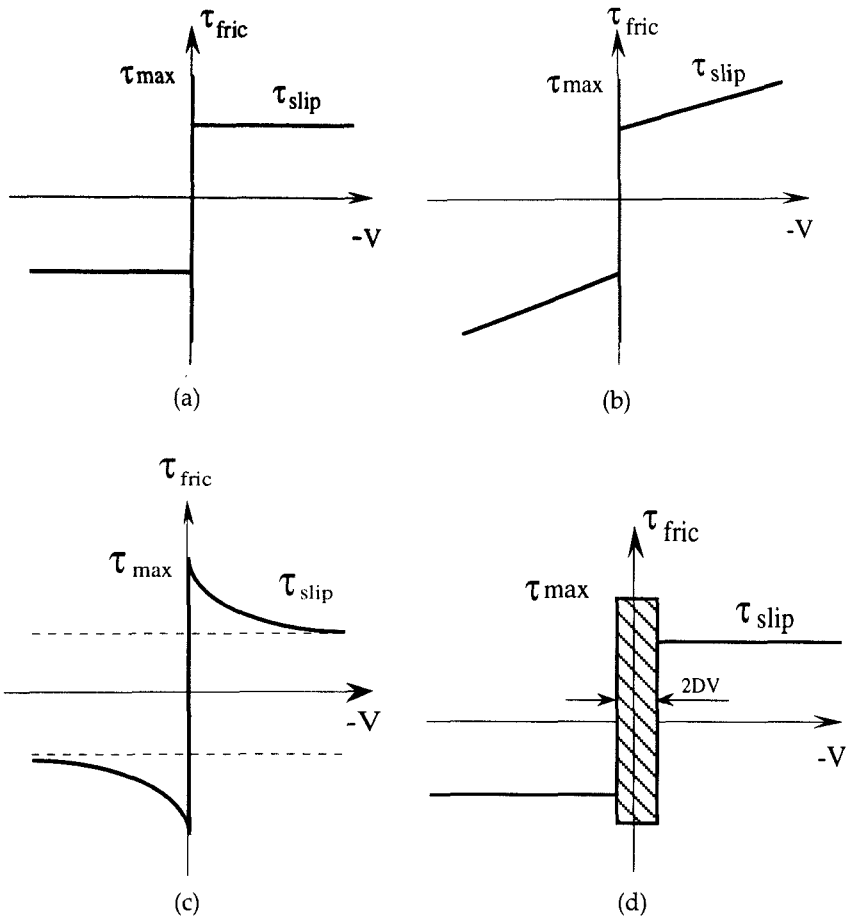

Figure 1. Commonly used stick-slip friction models. (a) Stiction/Coulomb Model. (b) Stiction, Coulomb plus Viscous Model. (c) Exponential Model. (d) Karnopp's Version of Stiction/Coulomb Model.

The slipping process is relatively complicated. Many factors affect the friction torque such as lubrication, velocity, position and forces orthogonal to the motion surface, and even the history of motion.[17] Based on the above factors, slipping torques are usually modeled as a linear combination of Coulomb torque, viscous torque, exponential torque,[2,18] and position and history dependent components.[6,17] Some commonly used friction models are shown in Figure 1a–1c.

All the proposed models have shown the common characteristic of the stick-slip friction: a significant change of friction magnitude in the zero-velocity vicinity in addition to the sign alternation. This behavior adversely affects the performance of mechanisms, and it is the major concern of the friction compensation.

Based on the facts that stick friction resists the applied torque, slipping friction dissipates kinetic energy and the assumption that the transition from stick process to slipping process is instantaneous. In general, friction torque can be formulated as:

$$\tau_{\text{fric}} = -\text{sgn}(v)\tau_{\text{slip}} - (1 - \text{abs}(\text{sgn}(v)))\tau_{\text{stick}}(\tau_{\text{appl}}) \quad (1)$$

where abs(v) gives the absolute value of v; sgn(v) is defined in Eq. (2); τ_{fric} is the friction torque; τ_{slip} is the magnitude of slipping torque (some commonly used models are shown in Table I); τ_{appl} is the applied joint torque; and τ_{stick} is the stiction torque given by Eq. (3).

$$\text{sgn}(v) = \begin{cases} +1 & v > DV > 0 \\ 0 & -DV \le v \le DV \\ -1 & v < -DV < 0 \end{cases} \quad (2)$$

$$\tau_{\text{stick}}(\tau_{\text{appl}}) = \begin{cases} \tau_{\text{appl}} & \text{abs}(\tau_{\text{appl}}) < \tau_{\max} \\ \tau_{\max} & \text{abs}(\tau_{\text{appl}}) \ge \tau_{\max} \end{cases} \quad (3)$$

Table I. Commonly used models of slipping friction.

Stiction/Coulomb Model	$\tau_{slip} = a$ where constant $a > 0$
Stiction, Coulomb plus Viscous Model	$\tau_{slip} = a + b\|v\|$ where constants $a, b > 0$
Exponential Model	$\tau_{slip} = \tau_{max} - \tau_a[1 - e^{-(\|v\|/v_0)}]$ where τ_{max} is the maximum static torque, constants τ_a, $v_0 > 0$
Position-Dependent Model (e.g.)	$\tau_{slip} = a + b \sin(cq + \theta)$ where a is the Coulomb friction torque, θ is constant and constants $a, b, c > 0$, $a > b$

where τ_{max} is the maximum static friction torque. *DV* is a positive number introduced by Karnopp in his friction model to specify the zero velocity zone. In that zone, all nonzero velocity will be considered as zero and stiction will be in effect.[11] The small zero-velocity zone in Karnopp's model surrounding $v = 0$ is necessary for numerical computation and digital implementation because an exact value of zero is hard to compute. The real stick-slip model is achieved when *DV* is taken to be zero. In this article, *DV* is taken to be zero for stability analysis. The stiction/Coulomb friction model with zero velocity zone is shown in Figure 1d.

2.2. System Equation

Due to the complexity of friction models in individual components, an aggregate friction model for each robot joint is considered. For an n dof rigid robot with stick-slip joint friction, its vectorial dynamic equation in terms of generalized coordinates and generalized forces is described by:

$$\mathbf{M}(\mathbf{q})\ddot{\mathbf{q}} + \mathbf{C}(\mathbf{q}, \dot{\mathbf{q}})\dot{\mathbf{q}} + \mathbf{G}(\mathbf{q}) = \Gamma_{appl} + \Gamma_{fric} \quad (4)$$

where

$\mathbf{M}(\mathbf{q}) \in \mathbf{R}^{n\times n}$	is the symmetric positive definite inertial matrix;
$\mathbf{C}(\mathbf{q}, \dot{\mathbf{q}})\dot{\mathbf{q}} \in \mathbf{R}^n$	is the vector defining Coriolis and centrifugal torques;
$\mathbf{G}(\mathbf{q}) \in \mathbf{R}^n$	is the vector defining gravity torques;
$\mathbf{q} \in \mathbf{R}^n$	is the vector representing the joint displacements;
$\dot{\mathbf{q}}, \ddot{\mathbf{q}} \in \mathbf{R}^n$	are the vectors representing, respectively, the first and second derivatives of $\mathbf{q}$;
$\Gamma_{appl} \in \mathbf{R}^n$	is the vector of input torques;
$\Gamma_{fric} \in \mathbf{R}^n$	is the vector of generalized joint friction torques, given by Eq. (5).

$$\Gamma_{fric} = \begin{bmatrix} -\text{sgn}(\dot{q}_1)\tau_{slip1} \\ -\text{sgn}(\dot{q}_2)\tau_{slip2} \\ \vdots \\ \vdots \\ -\text{sgn}(\dot{q}_n)\tau_{slipn} \end{bmatrix} + \begin{bmatrix} -(1 - \text{abs}(\text{sgn}(\dot{q}_1)))\tau_{stick1} \\ -(1 - \text{abs}(\text{sgn}(\dot{q}_2)))\tau_{stick2} \\ \vdots \\ \vdots \\ -(1 - \text{abs}(\text{sgn}(\dot{q}_n)))\tau_{stickn} \end{bmatrix} \quad (5)$$

where τ_{slipi} and τ_{stacki} are, respectively, the slipping and stiction torques of the ith joint. τ_{stacki} is given in Eq. (3), whereas τ_{slipi} depends on the selected slipping model.

3. A ROBUST CONTROLLER FOR POSITIONAL REGULATION

3.1. Assumptions

The maximum static torque at each joint is assumed to be a constant and exactly known.

3.2. Proposal of the Controller

Without loss of generality, the origin of the state space ($\mathbf{q} = 0$ and $\dot{\mathbf{q}} = 0$) is chosen as the desired reference position for the system given by Eq. (4). We propose the following control law:

$$\Gamma_{appl} = \mathbf{G}(\mathbf{q}) - \mathbf{K}_v\dot{\mathbf{q}} - \mathbf{K}_p\mathbf{q} - \Gamma_{non} \quad (6)$$

where:

$\mathbf{K}_v \in \mathbf{R}^{n\times n}$	is the positive definite diagonal matrix with derivative feedback gains;
$\mathbf{K}_p \in \mathbf{R}^{n\times n}$	is the positive definite diagonal matrix with proportional feedback gains;
$\mathbf{G}(\mathbf{q}) \in \mathbf{R}^n$	is the vector representing the feed-forward torques used to cancel the

gravitational effect, and can be expressed as $\mathbf{G}(\mathbf{q}) = [g_1, g_2, \cdots, g_n]^T$ (an algorithm to estimate $\mathbf{G}(\mathbf{q})$ is presented in the Appendix A);

$\Gamma_{non} \in \mathbf{R}^n$ is the vector representing the nonlinear friction compensator, and is defined by Eq. (7):

$$\Gamma_{non} = \begin{bmatrix} \tau_{ms1}\,\mathrm{Tanh}(\alpha_1 q_1) \\ \tau_{ms2}\,\mathrm{Tanh}(\alpha_2 q_2) \\ \vdots \\ \vdots \\ \tau_{msn}\,\mathrm{Tanh}(\alpha_n q_n) \end{bmatrix} \tag{7}$$

where the hyperbolic function $\mathrm{Tanh}(\alpha_i q_i) = (e^{\alpha_i q_i} - e^{-\alpha_i q_i})/(e^{\alpha_i q_i} + e^{-\alpha_i q_i})$; and $\tau_{msi} = \tau_{maxi} + \varepsilon_i$; α_i is a positive number used to adjust the steady-state error; τ_{maxi} is the maximum static friction torque of the ith joint; and ε_i is a positive number used to guarantee that the applied joint torque will always exceed the static friction torque and to ensure that the link is moving toward the desired position until its permitted error is reached. The control algorithm is illustrated in Figure 2.

3.3. Stability Theorem and Proof

Theorem 1: *The n-link robot system described in Eq. (4) is globally stable with the smooth nonlinear controller given by Eq. (6) and the steady-state error of each joint is bounded by q_{maxi}, which is given by the following equation:*

$$q_{maxi} = \frac{1}{2\alpha_i} \ln\left(1 + \frac{2\tau_{maxi}}{\varepsilon_i}\right) \tag{8}$$

where positive numbers α_i, ε_i and τ_{maxi} are given in Section 3.2.

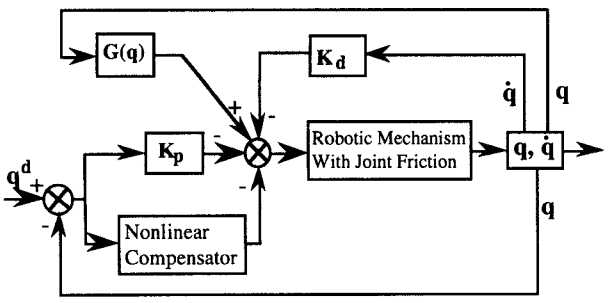

Figure 2. Block diagram of the control system.

Proof: Consider the Lyapunov function candidate:

$$V = \tfrac{1}{2}\dot{\mathbf{q}}^T\mathbf{M}\dot{\mathbf{q}} + \tfrac{1}{2}\mathbf{q}^T\mathbf{K}_p\mathbf{q} + \sum_{i=1}^{n} \frac{\tau_{msi}}{\alpha_i} \ln \frac{e^{\alpha_i q_i} + e^{-\alpha_i q_i}}{2} \tag{9}$$

It is easy to show that this Lyapunov function candidate is positive definite, continuous, and differentiable with respect to q_i and time t.

With the controller given by Eq. (6), the closed-loop system can be described as:

$$\mathbf{M}(\mathbf{q})\ddot{\mathbf{q}} + \mathbf{C}(\mathbf{q}, \dot{\mathbf{q}})\dot{\mathbf{q}} + \mathbf{G}(\mathbf{q}) = -K_v\dot{\mathbf{q}} - \mathbf{K}_p\mathbf{q} + \mathbf{G}(\mathbf{q}) - \Gamma_{non} + \Gamma_{fric} \tag{10}$$

The derivative of V along the system trajectory in Eq. (10) is obtained as:

$$\begin{aligned}
\dot{V} &= \dot{\mathbf{q}}^T\mathbf{M}\ddot{\mathbf{q}} + \mathbf{q}^T\mathbf{K}_p\dot{\mathbf{q}} + \tfrac{1}{2}\dot{\mathbf{q}}^T\dot{\mathbf{M}}\dot{\mathbf{q}} + \sum_{i=1}^{n} \tau_{msi}\tanh(\alpha_i q_i)\dot{q}_i \\
&= \dot{\mathbf{q}}^T(-\mathbf{C}(\mathbf{q}, \dot{\mathbf{q}})\dot{\mathbf{q}} - \mathbf{K}_v\dot{\mathbf{q}} - \mathbf{K}_p\mathbf{q} - \Gamma_{non} + \Gamma_{fric}) \\
&\quad + \mathbf{q}^T\mathbf{K}_p\dot{\mathbf{q}} + \tfrac{1}{2}\dot{\mathbf{q}}^T\dot{\mathbf{M}}\dot{\mathbf{q}} + \sum_{i=1}^{n} \tau_{msi}\,\mathrm{Tanh}(\alpha_i q_i)\dot{q}_i \\
&= \tfrac{1}{2}\dot{\mathbf{q}}^T(\dot{\mathbf{M}} - 2\mathbf{C}(\mathbf{q}, \dot{\mathbf{q}}))\dot{\mathbf{q}} - \dot{\mathbf{q}}^T\mathbf{K}_v\dot{\mathbf{q}} + \dot{\mathbf{q}}^T\Gamma_{fric} \\
&\quad + \left(\sum_{i=1}^{n} \tau_{msi}\,\mathrm{Tanh}(\alpha_i q_i)\dot{q}_i - \dot{\mathbf{q}}^T\Gamma_{non}\right) \\
&= -\dot{\mathbf{q}}_T\mathbf{K}_v\dot{\mathbf{q}} + \dot{\mathbf{q}}^T\Gamma_{fric} \\
&= -\dot{\mathbf{q}}^T\mathbf{K}_v\dot{\mathbf{q}} - \dot{\mathbf{q}}^T\left\{\begin{bmatrix} \mathrm{sgn}(\dot{q}_1)\tau_{slip1} \\ \mathrm{sgn}(\dot{q}_2)\tau_{slip2} \\ \vdots \\ \vdots \\ \mathrm{sgn}(\dot{q}_n)\tau_{slipn} \end{bmatrix}\right. \\
&\quad \left. + \begin{bmatrix} (1 - \mathrm{abs}(\mathrm{sgn}(\dot{q}_1)))\tau_{stick1} \\ (1 - \mathrm{abs}(\mathrm{sgn}(\dot{q}_2)))\tau_{stick2} \\ \vdots \\ \vdots \\ (1 - \mathrm{abs}(\mathrm{sgn}(\dot{q}_n)))\tau_{stickn} \end{bmatrix}\right\} \\
&= -\dot{\mathbf{q}}^T\mathbf{K}_v\dot{\mathbf{q}} - \sum_{i=1}^{n} \dot{q}_i\,\mathrm{sgn}(\dot{q}_i)\tau_{slipi} \\
&\quad - \sum_{i=1}^{n} \dot{q}_i(1 - \mathrm{abs}(\mathrm{sgn}(\dot{q}_i)))\tau_{stacki} \\
&= -\dot{\mathbf{q}}^T\mathbf{K}_v\dot{\mathbf{q}} - \sum_{i=1}^{n} \|\dot{\mathbf{q}}\|\tau_{slipi} \qquad (11) \\
&\le 0 \qquad (12)
\end{aligned}$$

where $\mathbf{K}_v$ is positive definite; $\tau_{slipi} \geq 0$; and $(\dot{\mathbf{M}} - 2\mathbf{C})$ is a skew symmetric matrix. During the derivation, the following equations are also used:

$$\dot{\mathbf{q}}^T(\dot{\mathbf{M}} - 2\mathbf{C})\dot{\mathbf{q}} = 0 \tag{13}$$

$$\sum_{i=1}^{n} \tau_{msi} \text{Tanh}(\alpha_i q_i)\dot{q}_i - \dot{\mathbf{q}}^T \Gamma_{non} = 0 \tag{14}$$

$$\dot{q}_i(1 - \text{abs}(\text{sgn}(\dot{q}_i))) = 0 \tag{15}$$

If $\dot{V} = 0$, then $q_i = 0$. Let $\mathbf{R}_v$ be the set of all points where $\dot{V} = 0$, and $\mathbf{E}$ be the largest invariant set in $\mathbf{R}_v$. Based on the fact that $\dot{V} \leq 0$ and $V \rightarrow \infty$ as $\|\mathbf{q}\| \rightarrow \infty$, all solutions of Eq. (10) will globally asymptotically converge to $\mathbf{E}$ as $t \rightarrow \infty$ by applying LaSalle's theorem. $\mathbf{R}_v$ can be described as:

$$\mathbf{R}_v = \{\mathbf{q} \in \mathbf{R}^n: \dot{\mathbf{q}} = 0\} \tag{16}$$

$\mathbf{E}$ is then determined by:

$$\begin{aligned}\mathbf{E} &= \{\mathbf{q} \in \mathbf{R}^n: \ddot{\mathbf{q}} = 0 \text{ and } \dot{\mathbf{q}} = 0\} \\ &= \{\mathbf{q} \in \mathbf{R}^n: \Gamma_{stick} - \mathbf{K}_p\mathbf{q} - \Gamma_{non} = 0\} \\ &= \{\mathbf{q} \in \mathbf{R}^n: |K_{pi}q_i + \tau_{msi} \text{Tanh}(\alpha_i q_i)| \\ &\quad \leq \tau_{maxi}, \text{ for } i = 1, \cdots, n\}\end{aligned} \tag{17}$$

The nonlinear inequality can be rewritten as:

$$K_{pi}|q_i| + \tau_{msi} \text{Tanh}(\alpha_i|q_i|) \leq \tau_{maxi} \tag{18}$$

because both $K_{pi}q_i$ and $\tanh(\alpha_i q_i)$ have the same sign as q_i. Note that the left-hand side of Eq. (18) becomes a monotonic function of $|q_i|$, so τ_{stick} reaches its maximum value τ_{maxi} only when $|q_i|$ reaches its maximum value. From Eq. (18), we have:

$$\tau_{msi} \text{Tanh}(\alpha_i|q_i|) \leq \tau_{maxi} \tag{19}$$

Solving Eq. (19), we get:

$$|q_i| \leq q_{maxi} \tag{20}$$

where:

$$q_{maxi} = \frac{1}{2\alpha_i} \ln \frac{\tau_{msi} + \tau_{maxi}}{\tau_{msi} - \tau_{maxi}} \tag{21}$$

Eq. (21) can be simplified to Eq. (8) by using the fact that $\tau_{msi} = \tau_{maxi} + \varepsilon_i$. So the largest invariant set $\mathbf{E}$ is bounded by q_{maxi}, which is a function of controller parameters α_i, ε_i and friction model parameter τ_{maxi}. Each joint displacement q_i will globally asymptotically converge to the invariant set with radius q_{maxi}. Thus, the steady-state error is bounded by q_{maxi} described by Eq. (8). ■

Remarks:

1. The radius of the invariant set depends on the design parameters α_i and ε_i. The maximum steady-state error, q_{maxi}, can be reduced by increasing either ε_i or α_i. Increasing ε_i means more actuator output, and possibly leads to saturation. On the other hand, increasing α_i will only change the shape of $\text{Tanh}(\alpha_i q_i)$, therefore enhancing the ability of the nonlinear compensator to overcome the friction without causing saturation. The plots of $\text{Tanh}(\alpha_i q_i)$ vs. q_i with the different values of α_i and the plot of slipping friction (Coulomb type) are shown in Figure 3, from which we can see that with a larger value of α_i, the nonlinear torque $\text{Tanh}(\alpha_i q_i)$ can exceed the Coulomb torque at a lower position value.

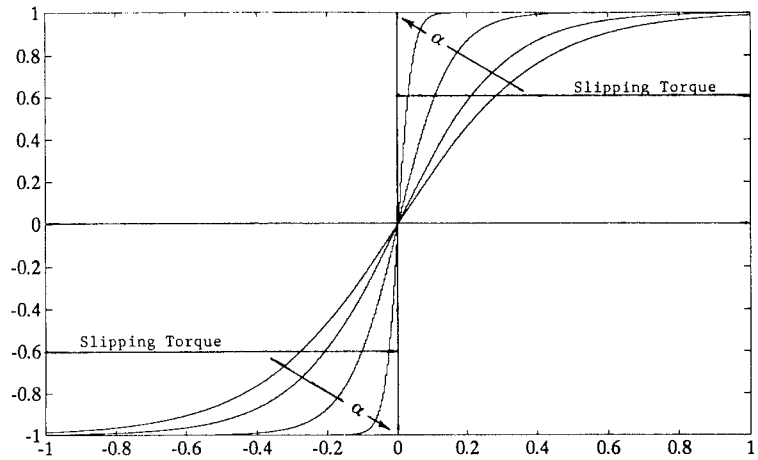

Figure 3. Plots of $\text{Tanh}(\alpha_i q_i)$ with different value of α_i.

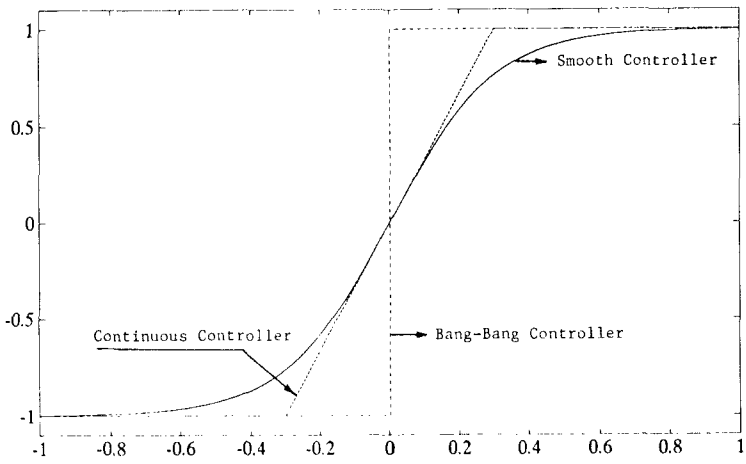

Figure 4. Schematic plots of $\tanh(\alpha_i q_i)$, bang-bang type controller, and continuous type controller.

2. When comparing the nonlinear compensator $\text{Tanh}(\alpha_i q_i)$ with the switch controller (bang-bang type) and the switch controller with boundary layer (continuous type), we note that the switch controller with boundary layer is a linear approximation of our nonlinear compensator while the bang-bang controller can be considered as an extreme case of the nonlinear compensator when asymptotic stability of the control system is achieved as $\alpha_i \to \infty$. The plots of $\text{Tanh}(\alpha_i q_i)$, the bang-bang type compensator, and the continuous compensator with boundary layer are shown in Figure 4.

3. The proposed nonlinear controller is smooth with respect to time t and joint displacement q_i. Thus the smooth input torques are ensured.

4. Within the invariant set (i.e., the required accuracy is reached), velocity is zero, so there will be no limit cycle generation.

The proposed time-invariant controller requires the experimental estimation of $\mathbf{G}(\mathbf{q})$, and the estimation must be updated if any link parameters change. Moreover, the controller is not suitable for trajectory tracking. In the following section, we develop a time-varying controller for robot trajectory tracking. Furthermore, the designed controller is robust with respect to the uncertain link parameters.

4. A ROBUST CONTROLLER FOR TRAJECTORY TRACKING

In this section, a time-varying smooth robust controller is proposed for robot tracking control. If the system parameters are exactly known, the resolved-acceleration method by Luh et al,[19] or a more general form, the "exact linearization" method,[20] can be used. Because we are considering the tracking control of uncertain robot manipulators, robust control approaches must be employed. In the following approach, we use the idea of sliding surface proposed by Slotine and Li.[21]

4.1. Assumptions

For the robot system in Eq. (4) with uncertain link parameters and unknown joint friction models, we have the following assumptions.

1. The upper bound of each uncertain parameter in the system is known.
2. The upper bound of the maximum static friction force and upper bounding function of the friction force at each internal joint are known.

4.2. Related Mathematical Properties

1. The following two fundamental properties of the Euclidean norms of vector will be used in the stability proof.

$$\|\mathbf{r}\| \le \sum_{i=1}^{n} |r_i| \tag{22}$$

$$\mathbf{r}^T\omega \le \|\mathbf{r}\|\|\omega\| \tag{23}$$

where $\mathbf{r} \in \mathbf{R}^n$ and $\omega \in \mathbf{R}^n$ are any two vectors, and $\|\cdot\|$ is defined as the Euclidean norm of a designated vector. We also define the corresponding norm of a matrix, say, $\mathbf{M}$, as:

$$\|\mathbf{M}\| = \sqrt{\lambda_{\max}(\mathbf{M}^T\mathbf{M})}$$

where $\lambda_{\max}(\cdot)[\lambda_{\min}(\cdot)]$ denotes the maximum (minimum) eigenvalue of a designated matrix. The same definitions of vector norm and matrix norm will be used throughout this article.

2. For any $r_i \neq 0$, and a, b, $t > 0$:

$$r_i\{\text{Tanh}[(a + bt)r_i]\} > 0 \tag{24}$$

$$|\text{Tanh}(r_i)| = \text{Tanh}(|r_i|) \tag{25}$$

4.3. Definitions of Related Terms

Before we propose the robust controller, some related terms are defined as following.

Let $\hat{\mathbf{M}}(\mathbf{q}) \in \mathbf{R}^{n\times n}$, $\hat{\mathbf{C}}(\mathbf{q}, \dot{\mathbf{q}}) \in \mathbf{R}^{n\times n}$, and $\hat{\mathbf{G}}(\mathbf{q}) \in \mathbf{R}^n$ denote the nominal or computed versions of $\mathbf{M}(\mathbf{q})$, $\mathbf{C}(\mathbf{q}, \dot{\mathbf{q}})$, and $\mathbf{G}(\mathbf{q})$, respectively. We define the correspondent uncertainty residue $\tilde{\mathbf{M}}(\mathbf{q}) \in \mathbf{R}^{n\times n}$, $\tilde{\mathbf{C}}(\mathbf{q}, \dot{\mathbf{q}}) \in \mathbf{R}^{n\times n}$, and $\tilde{\mathbf{G}}(\mathbf{q}) \in \mathbf{R}^n$, respectively, as:

$$\tilde{\mathbf{M}} = \hat{\mathbf{M}} - \mathbf{M} \tag{26}$$

$$\tilde{\mathbf{C}} = \hat{\mathbf{C}} - \mathbf{C} \tag{27}$$

$$\tilde{\mathbf{G}} = \hat{\mathbf{G}} - \mathbf{G} \tag{28}$$

The vectors of joint position error and velocity error are respectively defined by:

$$\mathbf{e} = \mathbf{q} - \mathbf{q}^d \tag{29}$$

$$\dot{\mathbf{e}} = \dot{\mathbf{q}} - \dot{\mathbf{q}}^d \tag{30}$$

where $\mathbf{q}^d \in \mathbf{R}^n$ and $\dot{\mathbf{q}}^d \in \mathbf{R}^n$ are the vectors describing the desired position trajectory.

Also, define $\mathbf{v}^d \in \mathbf{R}^n$ and $\dot{\mathbf{v}}^d \in \mathbf{R}^n$ as the following:

$$\mathbf{v} = \dot{\mathbf{q}}^d - \Lambda\mathbf{e} \tag{31}$$

$$\dot{\mathbf{v}} = \ddot{\mathbf{q}}^d - \Lambda\dot{\mathbf{e}} \tag{32}$$

and define $\mathbf{r} \in \mathbf{R}^n$ and $\dot{\mathbf{r}} \in \mathbf{R}^n$ by:

$$\mathbf{r} = \dot{\mathbf{q}} - \mathbf{v} = \dot{\mathbf{e}} + \Lambda\mathbf{e} \tag{33}$$

$$\dot{\mathbf{r}} = \ddot{\mathbf{q}} - \dot{\mathbf{v}} = \ddot{\mathbf{e}} + \Lambda\dot{\mathbf{e}} \tag{34}$$

where Λ is a constant diagonal matrix of positive gains.

4.4. The Proposed Controller

We propose the following tracking controller for the robot system from Eq. 4.

$$\Gamma_{\text{appl}} = \Gamma_{ff} - \mathbf{k}_{D0}\mathbf{r} - \rho_0\{\text{Tanh}[(a + bt)\mathbf{r}]\} \tag{35}$$

where:

Γ_{ff}	includes all the feedforward terms, and is defined by Eq. (36);
$\mathbf{k}_{D0} \in \mathbf{R}^{n\times n}$	is a positive diagonal linear feedback gain matrix;
$\mathbf{r} \in \mathbf{R}^n$	is defined in Eq. (33)
a and b	are positive constants used in the nonlinear compensator in Eq. (25);
ρ_0	is the scalar function that bounds the uncertainties, and is defined by Eq. (B1) in appendix B.

$$\Gamma_{ff} = \hat{\mathbf{M}}(\mathbf{q})\dot{\mathbf{v}} + \hat{\mathbf{C}}(\mathbf{q}, \dot{\mathbf{q}})\mathbf{v} + \hat{\mathbf{G}}(\mathbf{q}) \tag{36}$$

where $\dot{\mathbf{v}}$ and $\mathbf{v}$ are defined in Eqs. (31) and (32), respectively.

4.5. Stability Theorem and Proof

Theorem 2: *The robot system from Eq. (4) is globally asymptotically stable with the controller from Eq. (35), i.e., the trajectory tracking error converges to zero as* $t \to \infty$.

Proof: Substituting the controller from Eq. (35) into the system from Eq. (4) with Γ_{ff} defined in Eq. (36) gives:

$$\mathbf{M}\ddot{\mathbf{q}} + \mathbf{C}\dot{\mathbf{q}} + \mathbf{G} = \hat{\mathbf{M}}\dot{\mathbf{v}} + \hat{\mathbf{C}}\mathbf{v} + \hat{\mathbf{G}} - \mathbf{k}_{D0}\mathbf{r} - \rho_0\{\text{Tanh}[(a + bt)\mathbf{r}]\} + \Gamma_{\text{fric}}$$

Due to the fact $\ddot{\mathbf{q}} = \dot{\mathbf{r}} + \dot{\mathbf{v}}$ and $\dot{\mathbf{q}} = \mathbf{r} + \mathbf{v}$, the above equation can be rewritten as:

$$\mathbf{M}\dot{\mathbf{r}} + \mathbf{C}\mathbf{r} + \mathbf{k}_{D0}\mathbf{r} = \tilde{\mathbf{M}}\dot{\mathbf{v}} + \tilde{\mathbf{C}}\mathbf{v} + \tilde{\mathbf{G}} - \rho_0\{\text{Tanh}[(a + bt)\mathbf{r}]\} + \Gamma_{\text{fric}} \tag{37}$$

where $\tilde{\mathbf{M}}$, $\tilde{\mathbf{C}}$, and $\tilde{\mathbf{G}}$ are defined by Eqs. (26), (27), and (28), respectively.

Eq. (37) can be written as:

$$\mathbf{M}\dot{\mathbf{r}} + \mathbf{C}\mathbf{r} + \mathbf{k}_{D0}\mathbf{r} = -\rho_0\{\text{Tanh}[(a + bt)\mathbf{r}]\} + \omega_0 \tag{38}$$

where uncertainty vector ω_0 is defined by Eq. (B3) in appendix B.

Choose the Lyapunov function candidate:

$$V_0 = \frac{1}{2}\mathbf{r}^T\mathbf{M}\mathbf{r} \tag{39}$$

The derivative of V along the system trajectory of Eq. (38) is obtained as:

$$\begin{aligned}
\dot{V}_0 &= \mathbf{r}^T\mathbf{M}\dot{\mathbf{r}} + \frac{1}{2}\mathbf{r}^T\dot{\mathbf{M}}\mathbf{r} \\
&= -\mathbf{r}^T\mathbf{K}_{D0}\mathbf{r} + \mathbf{r}^T\{-\mathbf{C}\mathbf{r} - \rho_0\{\mathrm{Tanh}[(a+bt)\mathbf{r}]\} \\
&\quad + \omega_0\} + \frac{1}{2}\mathbf{r}^T\dot{\mathbf{M}}\mathbf{r} \\
&= -\mathbf{r}^T\mathbf{K}_{D0}r + r^T\left(\frac{1}{2}\dot{\mathbf{M}} - \mathbf{C}\right)\mathbf{r} \\
&\quad + \mathbf{r}^T\{-\rho_0\,\mathrm{Tanh}[(a+bt)\mathbf{r}] + \omega_0\} \\
&\le -\lambda_{\min}(\mathbf{K}_{D0})\|\mathbf{r}\|^2 + \mathbf{r}^T\{-\rho_0\,\mathrm{Tanh}[(a+bt)\mathbf{r}] + \omega_0\} \\
&\le -\lambda_{\min}(\mathbf{K}_{D0})\|\mathbf{r}\|^2 \\
&\quad - \rho_0\left\{\sum_{i=1}^{n} r_i\,\mathrm{Tanh}[(a+bt)r_i] - 1/\rho_0\sum_{i=1}^{n} r_i\omega_{0i}\right\} \\
&\le -\lambda_{\min}(\mathbf{K}_{D0})\|\mathbf{r}\|^2 \\
&\quad - \rho_0\left\{\sum_{i=1}^{n}\{|r_i|\,\mathrm{Tanh}[(a+bt)|r_i|]\} - \frac{\|\omega_0\|}{\rho_0}\|\mathbf{r}\|\right\} \\
&\le -\lambda_{\min}(\mathbf{K}_{D0})\|\mathbf{r}\|^2 \\
&\quad - \rho_0\left\{\sum_{i=1}^{n}|r_i|\,\mathrm{Tanh}[(a+bt)|r_i|] - \alpha_0\sum_{i=1}^{n}|r_i|\right\} \quad (40)
\end{aligned}$$

where $\alpha_0 = \|\omega_0\|/\rho_0$ (obviously, $0 \le \alpha_0 < 1$, according to (B2)).

It is clear from Eq. (40) that $\dot{V}_0 \le 0$ as long as the following condition is satisfied.

$$\sum_{i=1}^{n}|r_i|\,\mathrm{Tanh}[(a+bt)|r_i|] - \alpha_0\sum_{i=1}^{n}|r_i| \ge 0$$

i.e.,

$$|r_i|\,\mathrm{Tanh}[(a+bt)|r_i|] - \alpha_0|r_i| \ge 0$$

Solving the above inequality gives:

$$|r_i| \ge \gamma_0 \quad (41)$$

where:

$$\gamma_0 = \frac{1}{2(a+bt)}\ln\left(\frac{1+\alpha_0}{1-\alpha_0}\right). \quad (42)$$

In the above derivation, the properties from Eqs. (22)–(25) and $\mathbf{r}^T(\dot{\mathbf{M}} - 2\mathbf{C})\mathbf{r} = 0$ have been used. From the result of Eqs. (40) and (42), r_i will converge to a closed ball centered at the origin with a radius of γ_0 as long as Eq. (41) is satisfied. Furthermore, it can be easily shown from Eq. (42) that as $t \to \infty$, $\gamma_0 \to 0$. Therefore, as $t \to \infty$, $\dot{V}_0 \le 0$ and $\dot{V}_0 = 0$ only when $\mathbf{r} = 0$. Hence, it can be concluded that $\mathbf{r}$ asymptotically converges to zero as $t \to \infty$.

It is clear from Eq. (42) that a larger value of a will result in smaller value of γ_0 and a larger value of b will result in a faster convergence of γ_0. So, a and b can be adjusted to achieve the desired performance.

We now study the rate of convergence of $\mathbf{r}_i$ as $t \to \infty$. From Eq. (39):

$$\lambda_{\min}(\mathbf{M})\|\mathbf{r}\|^2 \le 2V_0 \le \lambda_{\max}(\mathbf{M})\|\mathbf{r}\|^2 \quad (43)$$

By using Eq. (43), we can derive the following from Eq. (40) when the inequality in Eq. (41) is satisfied:

$$\dot{V}_0 \le -2\eta V_0 \quad (44)$$

where $\eta = \lambda_{\min}(\mathbf{K}_{D0})/\lambda_{\max}(\mathbf{M})$
Integrating both sides of Eq. (44) with respect to the time gives:

$$V_0 \le \exp(-2\eta t)V_0(t_0)$$

By using Eq. (39), we can further derive that:

$$\|\mathbf{r}(t)\| \le \exp(-\eta t)\sqrt{\frac{V_0(t_0)}{\lambda_{\min}(\mathbf{M})}} \quad (45)$$

So $\mathbf{r}_i$ exponentially converges to the closed ball centered at the origin with a radius of γ_0 at least at a rate of η, meanwhile, γ_0 linearly converges to zero as $t \to \infty$. As shown in reference 22, if $\mathbf{r} \to \mathbf{0}$, then $\mathbf{e}$ and $\dot{\mathbf{e}}$ will converge to zero at $t \to \infty$. Therefore, asymptotic stability of the closed-loop system is achieved. ■

Remarks

1. The smoothness of the proposed time-varying controller with respect to time is still ensured.[23]

2. The proposed controller is not an adaptive one, however, it is time variant. Thus it can ensure asymptotic stability of the closed-loop system. By setting $\dot{\mathbf{q}}^d$ and $\ddot{\mathbf{q}}^d = 0$, the tracking problem changes to a regulation problem. Therefore, asymptotic stability can be achieved for the positional regulation.

3. Only practical stability (see ref. 24 for the definition) will be achieved by dropping the bt term in the proposed controller (Eq. (35)).

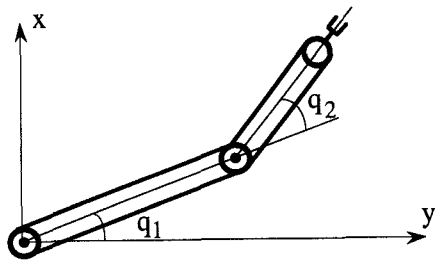

Figure 5. Schematic diagram of the two-link manipulator.

5. NUMERICAL SIMULATIONS

To illustrate the effectiveness of the proposed controllers, two cases of numerical simulations have been performed on a two-link robot (shown in Fig. 5) with internal joint stick-slip friction. In the first case, the time-invariant controller is applied to the two-link robot to perform a positional regulation task, while in the second case, the time-varying robust controller is implemented for the robot to perform a positional tracking task. The numerical simulations are performed on a PC 386 by using a simulation software implementing the Runge-Kutta integration algorithm.

The parameters of each link are: $m_1 = 4.0$(kg), $m_2 = 2.0$(kg); $l_1 = 0.5$(M), $l_2 = 0.35$(M). Karnopp's model is used for numerical simulations. *DV* is chosen to be 10^{-7} by considering both the availability of resolution of the real physical sensors and accuracy of the numerical simulation.

5.1. Case 1: Positional Regulation

Theoretically, control parameter ε_i in the position regulation controller can be any arbitrary positive number without affecting system stability, but ε_i should be chosen properly in simulation by considering both overshoot avoidance and convergence speed. The control parameter α_i is assigned to be 10^8 according to the Eq. (12).

The slipping torque of the exponential-plus-viscous friction model is described as:

$$\tau_{\text{slip}i} = \tau_{\text{max}i} - \tau_{ai}[1 - e^{-(|\dot{q}_i|/\dot{q}_{0i})}] + k_{vi}|\dot{q}_i| \quad i = 1, 2 \tag{46}$$

Table II. Model parameters.

Link	τ_{max}(N · M)	τ_a(N · M)	$\dot{q}_0$(rad/s)	k_v
1	1.0	0.5	10	5.0
2	0.75	0.325	10	5.0

Table III. Controller parameters.

	ε	α	k_p	k_v
1	0.04	10^8	41.9	30
2	0.02	10^8	40.1	30

The parameters of the dynamic model and the controller used in this case are shown in Tables II and III, respectively. The value of the maximum static torque of each joint is assumed to be constant and exactly known in this case. The initial configuration of the robot is:

$$\{q_1 = 1.0,\ v_1 = 0,\ q_2 = 0.65 \text{ and } v_2 = 0\}$$

It is not difficult to show that k_{p1} and k_{p2} will not saturate the actuators when the links are at the extreme position with allowed error. Thus the nonlinear compensator can exert torque to drive the link to its desired position at low velocity where proportional feedback is too weak to overcome the friction torque. Figure 6 shows that unsatisfactory steady-state error remains in each link when the two-link robot system is controlled without the nonlinear friction compensation torque. The positioning error of each link is greatly reduced when the nonlinear compensator is in effect. A close-up of the simulation of q_1 and q_2 between 4.5 s and 4.9 s is shown in Figure 7.

The joint velocity and displacement of link 1 and 2 throughout the whole simulation are shown in Figures 8 and 9. No position and velocity chattering are observed.

The small jumps of applied torques of link 1 and link 2 around $t = 4.7$ s (Figs. 10 and 11) are caused by the truncation of nonzero-velocity to zero-velocity when using Karnnop's Model. This will not happen if an analog controller is implemented. The jumps of the friction torque at the same time (Figs. 12 and 13) are induced by the dropping of Coulomb friction torque when zero-velocity zone is reached.

5.2. Case 2: Positional Tracking

To test the robustness of the time-varying controller in Eq. (35) with respect to the uncertain link parameters and the unknown friction model, we assume that the actual value of each link mass is unavailable for controller design, and both the maximum static friction forces and slipping torque at each joint are position-dependent and unknown to the design.

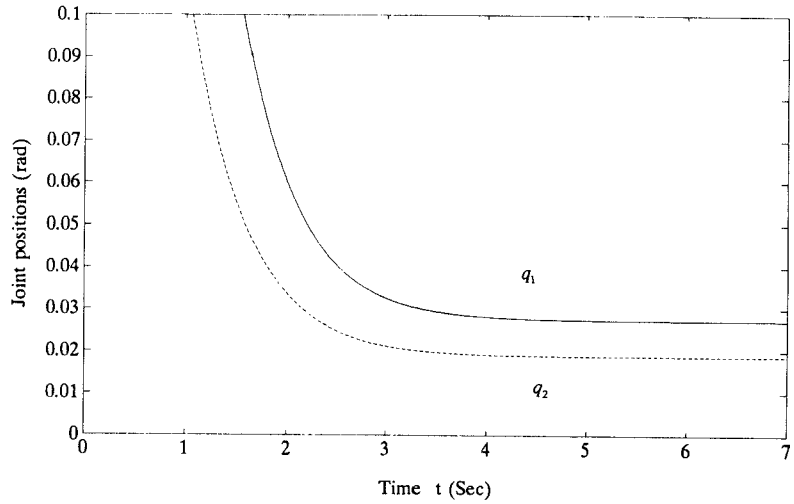

Figure 6. A close-up of joint positions without nonlinear compensator.

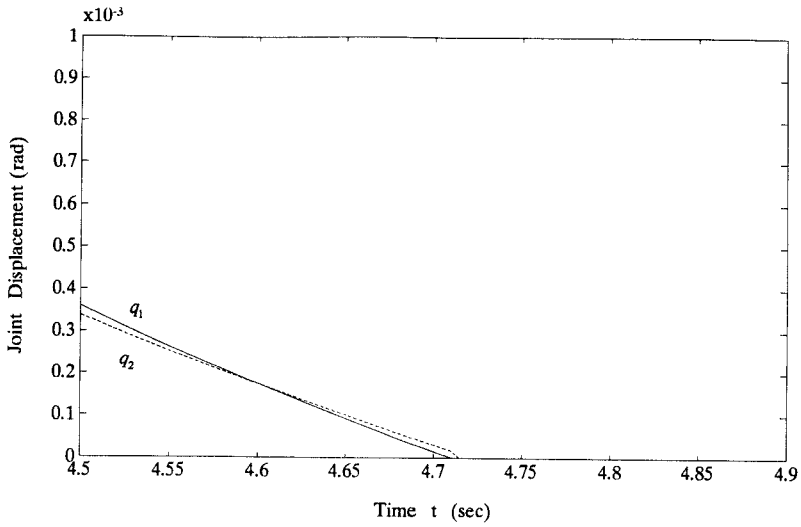

Figure 7. A close-up of joint positions with nonlinear compensator.

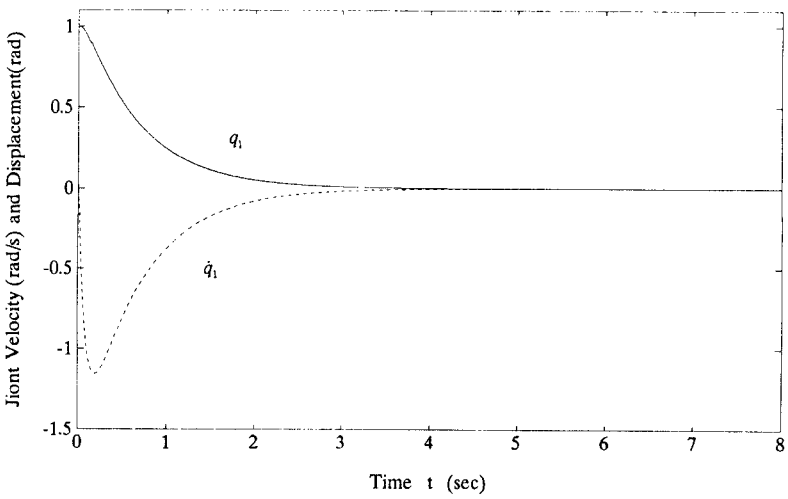

Figure 8. Joint velocity and position of link 1 with nonlinear compensator.

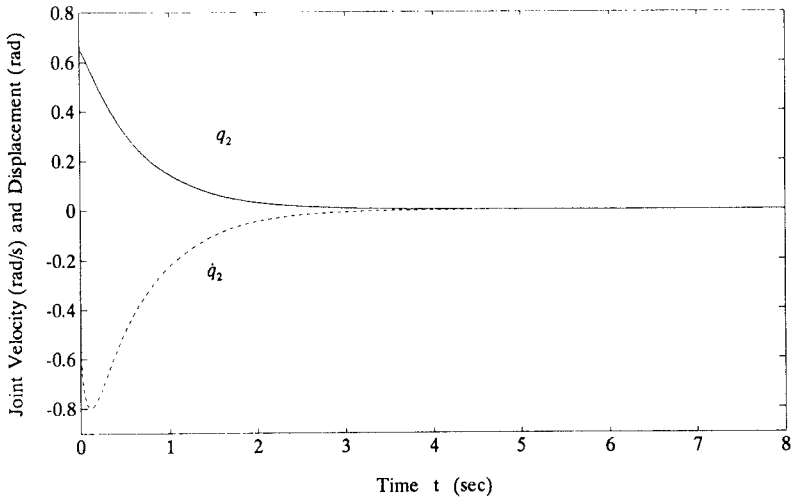

Figure 9. Joint velocity and position of link 2 with nonlinear compensator.

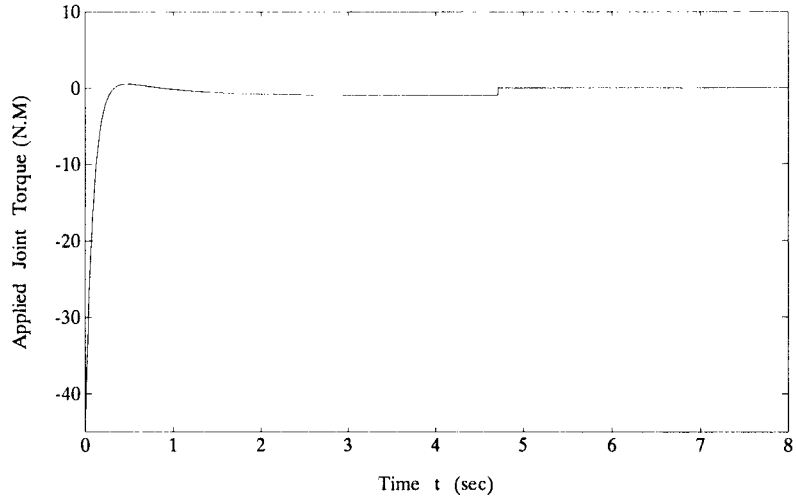

Figure 10. Applied torque on Joint 1.

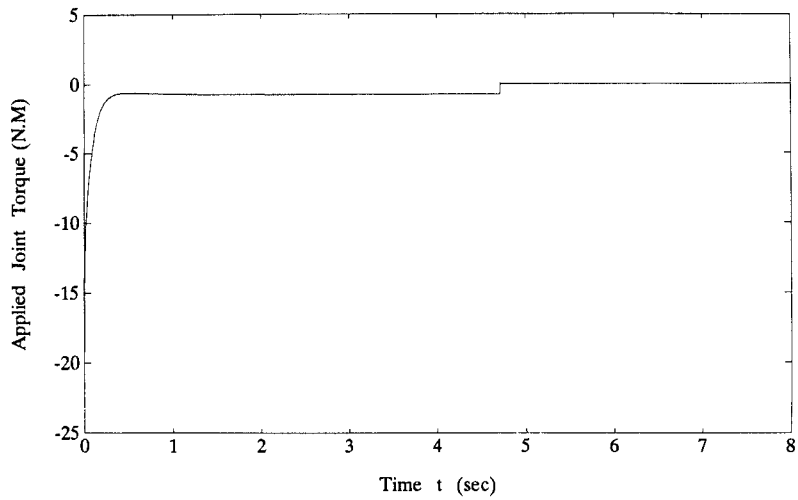

Figure 11. Applied torque on Joint 2.

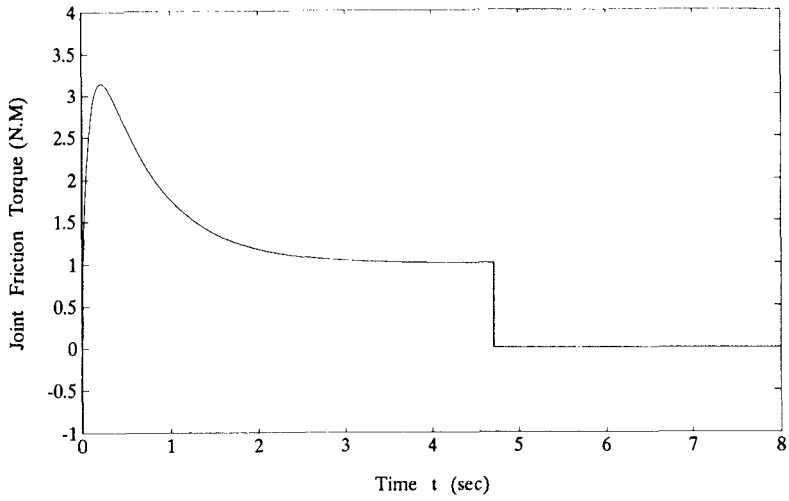

Figure 12. Joint friction torque of link 1.

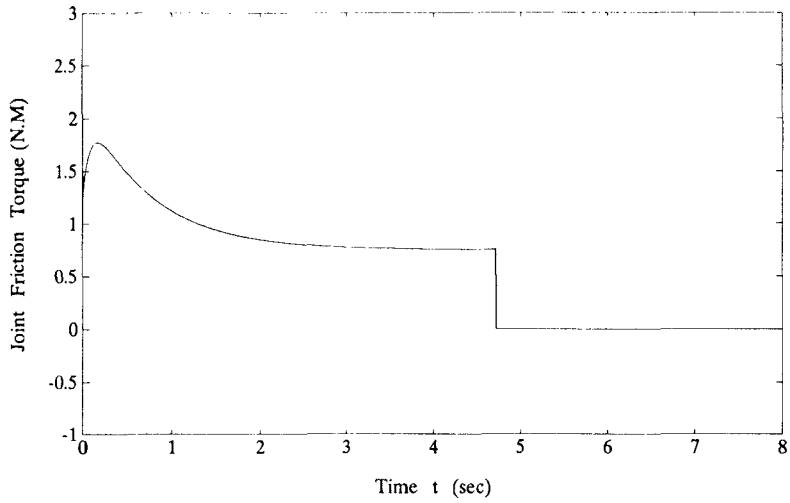

Figure 13. Joint friction torque of link 2.

However, the upper bounds for uncertain parameters, the upper bounds for maximum static friction forces, and the upper bounding function for the slipping friction are exactly known. The robot manipulator is required to follow a desired trajectory described in joint space as shown in Figure 14 (desired joint displacement) and Figure 15 (desired joint velocity). From Figure 15, we can see that both joints will pass through the zero joint velocity zones. Therefore, we have chances to demonstrate that the proposed controller can overcome the joint stiction without chattering.

The models for the maximum static friction forces and slipping torques are given respectively in Eqs. (47) and (48) with the model parameters shown in Table IV. The estimated values of the link masses are given by $\hat{m}_1 = 6.0$ (kg), $\hat{m}_2 = 3.0$ (kg).

$$\tau_{\text{max}i} = \tau_{\text{m}0i} + a_{0i}\sin(b_{0i}q_i + \theta_{0i}) \qquad i = 1, 2 \tag{47}$$

$$\tau_{\text{slip}i} = \tau_{bi} + \tau_{ai}[1 - e^{-(\|\dot{q}_i\|/\dot{q}_{0i})}] + k_{vi}\|\dot{q}_i\| + a_i\sin(b_iq_i + \theta) \qquad i = 1, 2 \tag{48}$$

The controller gains are given as the following: $a = 100$; $b = 10$; $\Lambda = \text{diag}[100, 100]$ and $\mathbf{K}_D = \text{diag}[30, 20]$. The coefficients in the bounding function $\rho_0(\mathbf{q}, \mathbf{q}^d, \dot{\mathbf{q}}, \dot{\mathbf{q}}^d)$ from Eq. (B1) are shown in Table V. We noticed that joint displacement q_i presents in $\tilde{\mathbf{M}}$, $\tilde{\mathbf{C}}$, and $\tilde{\mathbf{G}}$ in forms of $\cos(q_i)$ and $\sin(q_i)$, the magnitudes of which are bounded by 1, thus the

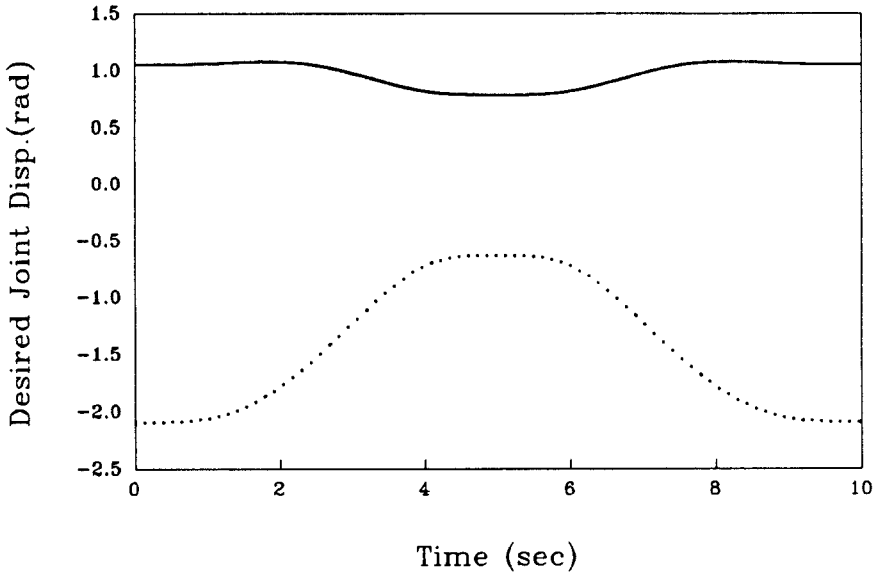

Figure 14. Desired joint displacements (solid line joint 1; dashed line joint 2).

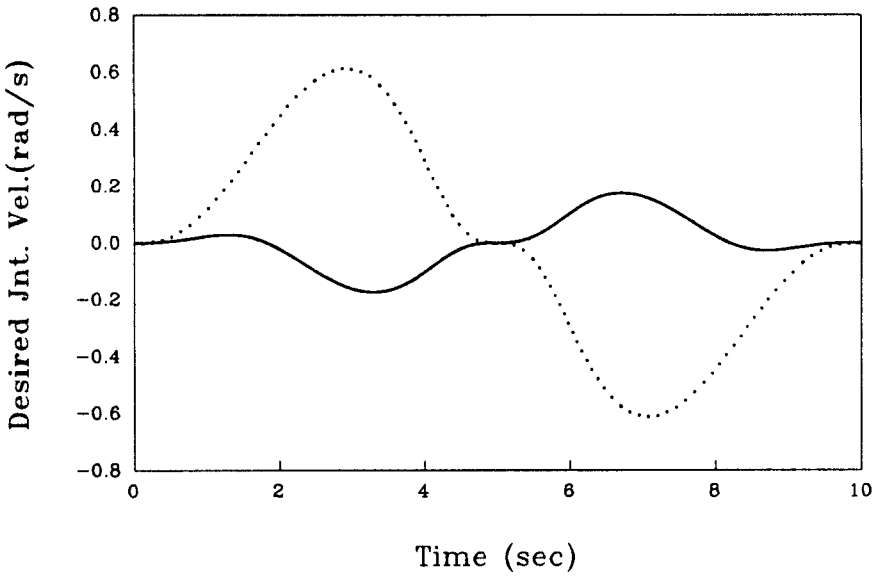

Figure 15. Desired joint velocity (solid line joint 1; dashed line joint 2).

Table IV. Friction model parameters.

Link	τ_{m0i}(N · M)	a_{0i}	b_{0i}	θ_{0i}(rad)	$\dot{q}_{0i}$(rad/s)	τ_{ai}(N · M)	τ_{bi}(N · M)	k_{vi}	a_i	b_i	θ_i(rad)
$i = 1$	1	0.2	10	0.05	0.05	0.5	0.5	0.2	0.05	25	0.05
$i = 2$	0.75	0.15	5	0.025	0.05	0.325	0.35	0.1	0.035	20	0.025

Table V. Coefficients used in bounding function.

β_1	β_2	β_3	ξ_1'
2	2	20	$1.3 + 1.1\|\mathbf{q}\|$

coefficients in Table V can be simply defined as constants by taking the corresponding upper bounds of $\cos(q_i)$ and $\sin(q_i)$.

As shown in Figures 16–19, the robot manipulator follows the desired trajectory precisely even under the adverse effects of uncertain robot link param-

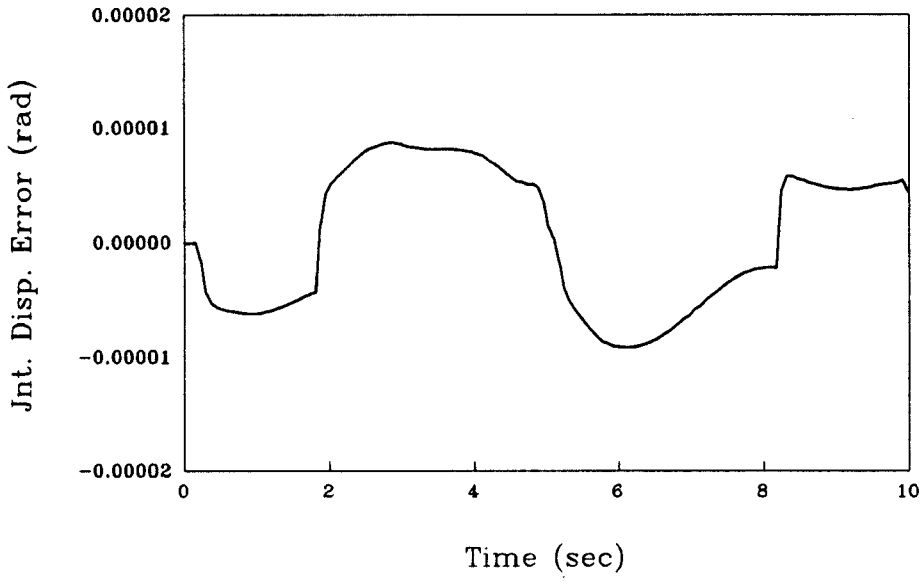

Figure 16. Position error of joint 1.

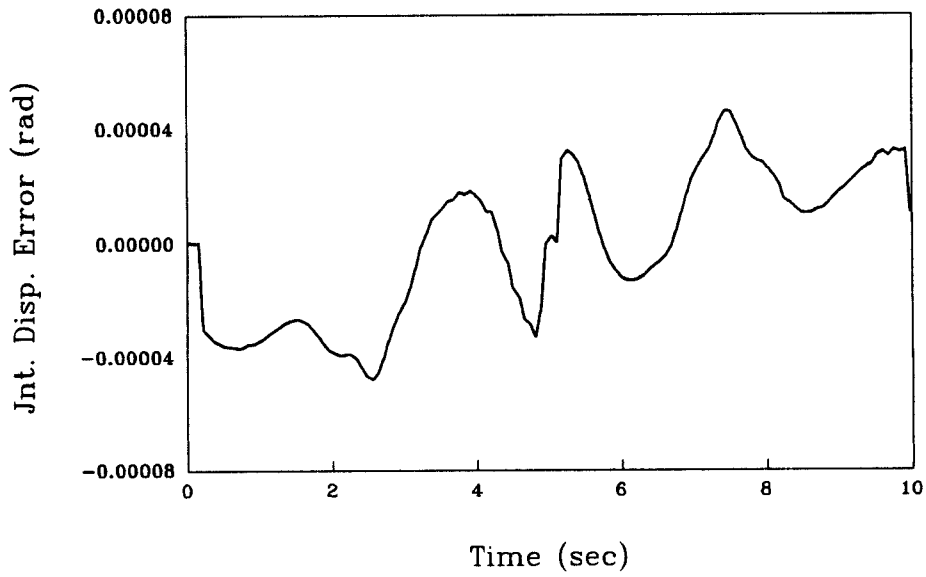

Figure 17. Position error of joint 2.

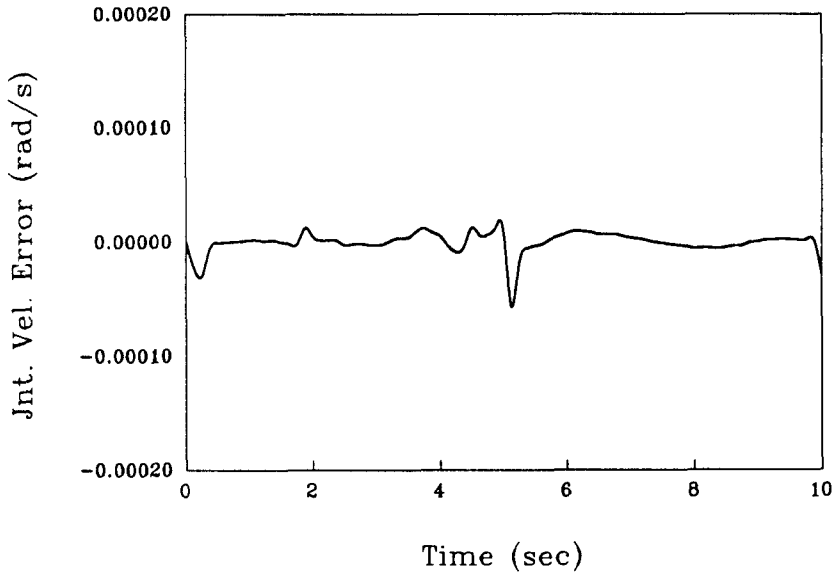

Figure 18. Velocity error of joint 1.

eters and the unknown joint friction models. Furthermore, the applied torques are smooth (as shown in Figs. 20 and 21). Moreover, no chattering is observed near the zero velocity zone around t = 5 s when the controller is overcoming the stiction force. In addition, the position-dependent joint friction torques are shown in Figs. 22 and 23.

6. CONCLUSIONS

In this article, we have proposed two new smooth robust nonlinear controllers, respectively, for positional regulation and tracking of rigid robot manipulators with internal joint stick-slip friction. In both cases, smooth and robust control has been achieved with global stability. Furthermore, the time-varying robust tracking controller guarantees the global asymptotic stability of the closed-loop system. The proposed controllers are continuously differentiable with respect to time and joint displacements. This guarantees that no extra acceleration disturbances will be introduced to the robot system and the unsmooth behavior (e.g., limit cycle, jerk discontinuity) will be eliminated. Both theoretical analysis and nu-

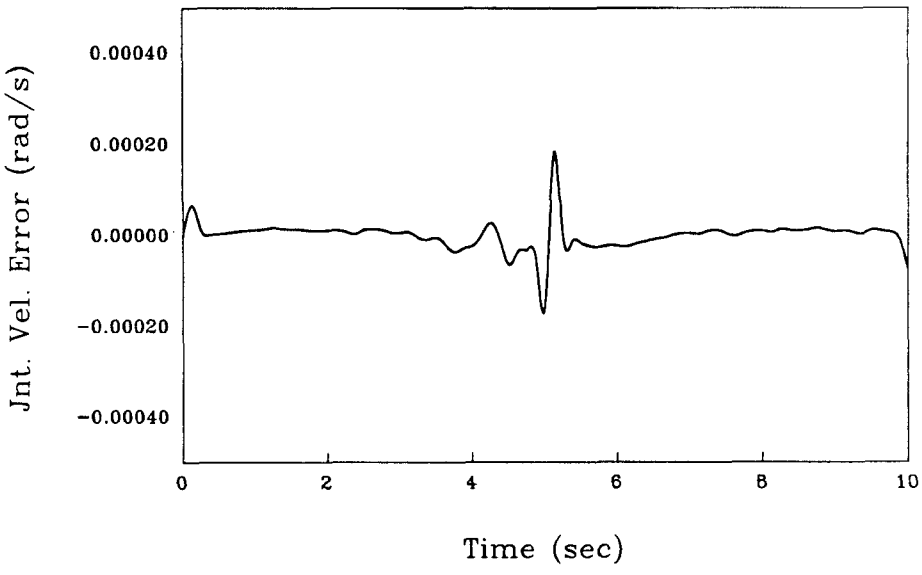

Figure 19. Velocity error of joint 2.

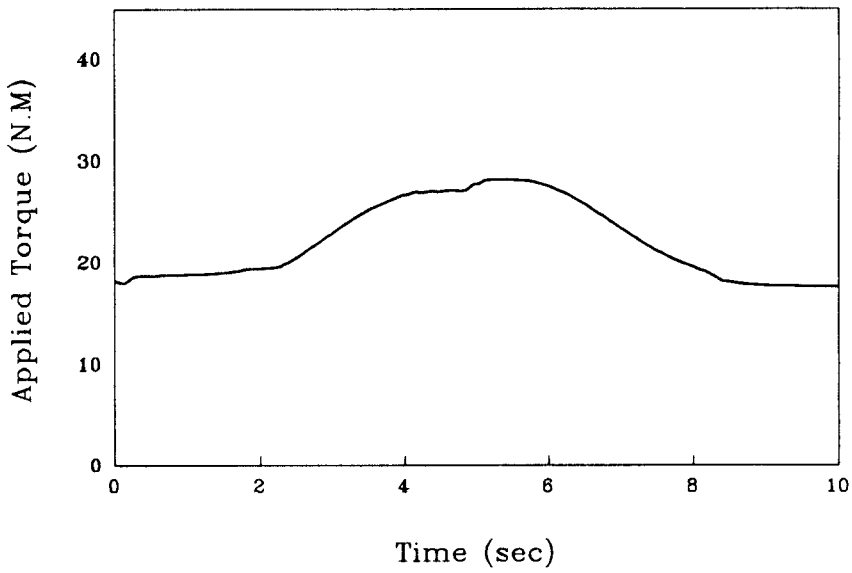

Figure 20. Applied torque on joint 1.

merical simulation have shown that the friction compensation is robust with respect to the character of friction torques. Moreover, the positional tracking controller is also insensitive to the variations of uncertain robot link parameters.

The proposed novel controllers are closely related to bang-bang controllers and continuous type controllers with boundary layers. In fact, the continuous type controller can be considered as a linear approximation of the proposed time-invariant controller, while if we choose either a or $b \to \infty$, then the proposed controllers would become the bang-bang-type controllers.

An interesting problem is to develop a controller for the robot system with internal joint stick-slip friction and the dry friction caused by the interaction between the robot's end-effector and the environment.

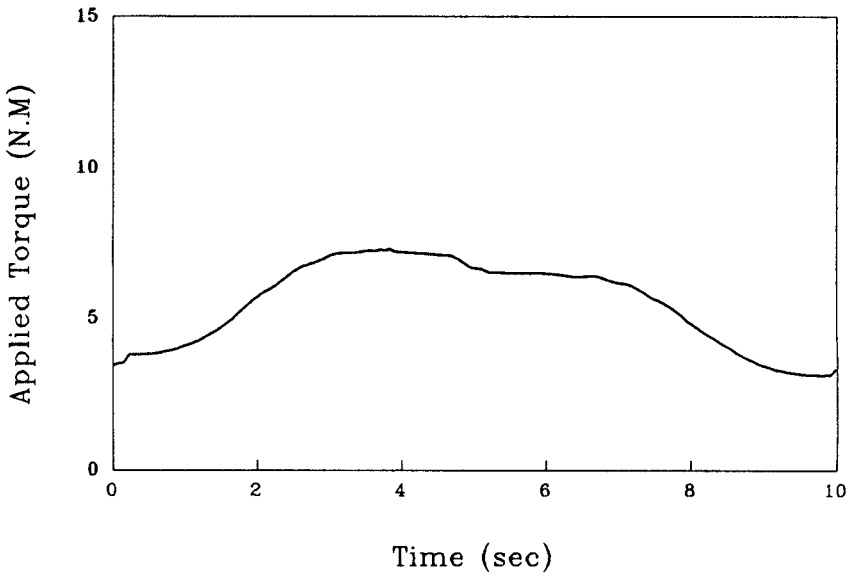

Figure 21. Applied torque on joint 2.

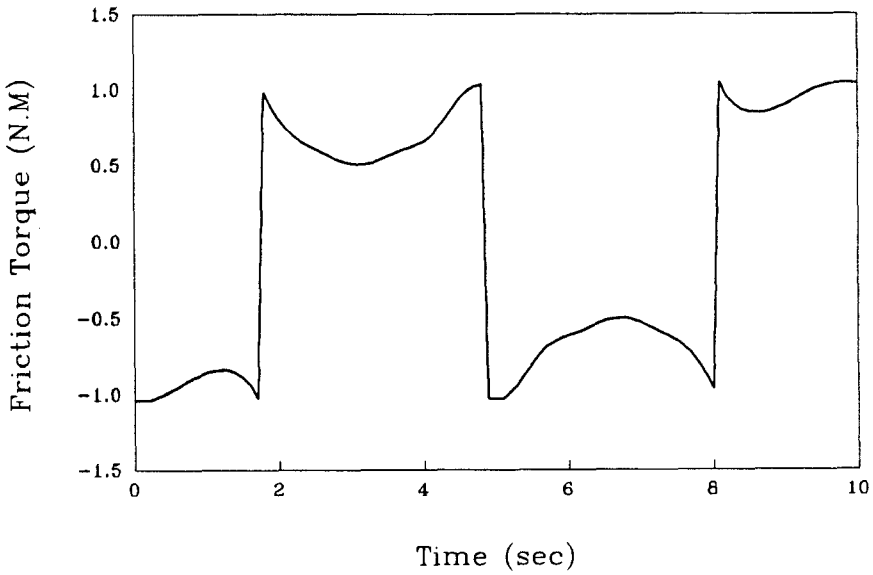

Figure 22. Friction torque of joint 1.

APPENDIX A: ALGORITHM TO ESTIMATE G(q)

At static state, Eq. (4) can be simplified to $\mathbf{G}(\mathbf{q}) = \Gamma_{appl} - \Gamma_{stick}$. In spite of the fact that $\mathbf{G}(\mathbf{q})$ is a nonlinear function of joint variables, the static-state equations are linear in terms of unknown coefficients of known functions of joint variables.[22] By defining each unknown coefficient as a new separate parameter, a linear relationship is achieved:

$$\mathbf{G}(\mathbf{q}) = \Phi(\mathbf{q})\Psi = \Gamma_{appl} - \Gamma_{stick} \qquad \text{(A1)}$$

where $\Phi(\mathbf{q}) \in \mathbf{R}^{n \times n}$ is the matrix of known functions of joint displacements, and $\Psi \in \mathbf{R}^n$ is the vector of the unknown parameters.

For example, consider the two-link robot shown in Figure 5, with a point mass located at the distal end of each link. The equation governing the static state is:

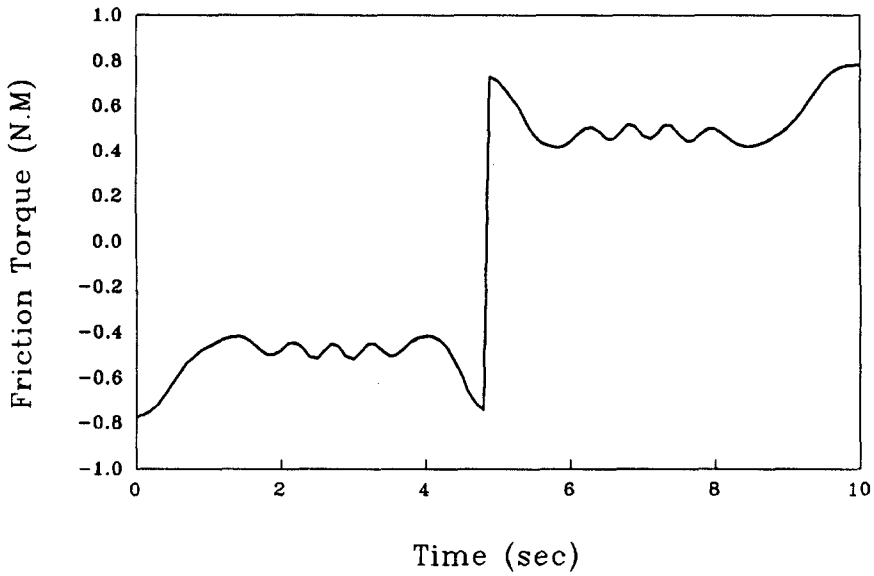

Figure 23. Friction torque of joint 2.

$$\begin{bmatrix} m_{12}l_1 g\cos(q_1) + m_2 l_2 g\cos(q_1 + q_2) \\ m_2 l_2 g\cos(q_1 + q_2) \end{bmatrix} = \begin{bmatrix} \tau_{appl1} - \tau_{stick1} \\ \tau_{appl2} - \tau_{stick2} \end{bmatrix} \quad \text{(A2)}$$

where $m_{12} = m_1 + m_2$ and m_1, m_2, l_1, l_2 are link mass and link length of link 1 and 2, respectively. In this case, $m_{12}l_1 g$ and $m_2 l_2 g$ are unknown. By defining $m_{12}l_1 g = \psi_1$ and $m_2 l_2 g = \psi_2$, a linear relationship can be achieved, i.e.,

$$\begin{bmatrix} \phi_1 & \phi_2 \\ 0 & \phi_2 \end{bmatrix} \begin{bmatrix} \psi_1 \\ \psi_2 \end{bmatrix} = \begin{bmatrix} \tau_{appl1} - \tau_{stick1} \\ \tau_{appl2} - \tau_{stick2} \end{bmatrix} \quad \text{(A3)}$$

where $\phi_1 = \cos(q_1)$ and $\phi_2 = \cos(q_1 + q_2)$.

Certain joint configurations can be chosen to ensure that the matrix $\Phi(\mathbf{q})$ is nonsingular. We can experimentally obtain the maximum value of the applied torque, τ_{mai}, to maintain the static state of each joint independently at the joint configuration. Ψ can be solved from Eq. (A1) at the critical (breakaway) state with the prior information of the maximum static torque of each joint:

$$\Psi = \Phi(\mathbf{q})^{-1}(\Gamma_{ma} - \Gamma_{max}) \quad \text{(A4)}$$

where Γ_{ma} and $\Gamma_{max} \in \mathbf{R}^n$ are the vectors representing the maximum applied torques and maximum static torques, respectively.

APPENDIX B: DEFINITION OF THE UNCERTAINTY BOUNDING FUNCTION

It is clear to show that the following hold based on assumptions 1–2 given in Section 4.1. There always exists a positive scalar function $\rho_0(\mathbf{q}, \mathbf{q}^d, \dot{\mathbf{q}}, \dot{\mathbf{q}}^d)$ defined by:

$$\rho_0(\mathbf{q}, \mathbf{q}^d, \dot{\mathbf{q}}, \dot{\mathbf{q}}^d) = \beta_1(\mathbf{q})\|\dot{\mathbf{v}}\| + \beta_2(\mathbf{q})\|\dot{\mathbf{q}}\|\|\mathbf{v}\| + \beta_3(\mathbf{q}) + \xi_1(\mathbf{q}, \dot{\mathbf{q}}) \quad \text{(B1)}$$

such that for all $\mathbf{q} \in \mathbf{R}^n$, $\dot{\mathbf{q}} \in \mathbf{R}^n$, and $t \in \mathbf{R}$;

$$\rho_0(\mathbf{q}, \mathbf{q}^d, \dot{\mathbf{q}}, \dot{\mathbf{q}}^d) > \|\omega_0\| \quad \text{(B2)}$$

where ω_0 is the uncertainty with regard to the position controller, and is defined as:

$$\omega_0 = \tilde{\mathbf{M}}\dot{\mathbf{v}} + \tilde{\mathbf{C}}\mathbf{v} + \tilde{\mathbf{G}} + \Gamma_{fric} \quad \text{(B3)}$$

and positive scalar functions $\beta_1(\mathbf{q})$, $\beta_2(\mathbf{q})$, $\beta_3(\mathbf{q})$, and $\xi_1(\mathbf{q}, \dot{\mathbf{q}})$ are defined so that:

$$\beta_1(\mathbf{q}) = k_1\|\tilde{\mathbf{M}}\| \quad \text{(B4)}$$

$$\beta_2(\mathbf{q})\|\dot{\mathbf{q}}\| = k_2\|\tilde{\mathbf{C}}\| \quad \text{(B5)}$$

$$\beta_3(\mathbf{q}) = k_3\|\tilde{\mathbf{G}}\| \quad \text{(B6)}$$

$$\xi_1(\mathbf{q}, \dot{\mathbf{q}}) = k_4\|\Gamma_{fric}\| \quad \text{(B7)}$$

where constants k_1, k_2, k_3, and $k_4 > 1$. The definitions in Eqs. (B4)–(B7) guarantee the satisfaction of the inequality in Eq. (B2) and ensure ρ_0 and $\|\omega_0\|$ will have the same order as $t \to \infty$ if the uncertainty goes to infinity.

In cases when only velocity-dependent viscous friction presents at each internal joint, ξ_1 defined in Eq. (B7) can be chosen as:

$$\xi_1 = \xi_1'\|\dot{\mathbf{q}}\|$$

where $\xi_1' > \mu_{jmax}$, with μ_{jmax} is the maximum value of the coefficients of slipping friction of the internal joints.

REFERENCES

1. A. Gogoussis and M. Donath, "Coulomb friction joint and drive effects in robot mechanisms," *IEEE International Conference on Robotics and Automation*, 1987, Vol. 2, pp. 828–836.
2. B. Armstrong, "Friction: Experimental determination, middling and compensation," *IEEE International Conference on Robotics and Automation*, 1988, Vol. 3, pp. 1422–1427.
3. C. Canudas de Wit et al. "Adaptive friction compensation in robot manipulators: Low-velocities," *IEEE International Conference on Robotics and Automation*, 1989, pp. 1352–1357.
4. P. Dupont, "Friction modeling in dynamic robot simulation," *IEEE International Conference on Robotics and Automation*, 1990, pp. 1370–1376.
5. W. S. Newman and G. D. Glosser, "The detrimental effect of friction on space microgravity robotics," *IEEE International Conference on Robotics and Automation*, 1992, pp. 1436–1441.
6. S. C. P. Gomes and J. P. Chretein, "Dynamic modeling and friction compensated control of a robot manipulator joint," *IEEE International Conference on Robotics and Automation*, 1992, Vol. 3, pp. 1429–1435.
7. P. Dupont, "The effect of Coulomb friction on the existence and uniqueness of the forward dynamics problems," *IEEE International Conference on Robotics and Automation*, 1992, pp. 1442–1447.
8. C. Radclitte and S. Southward, "A property of stick-slip friction models which promotes limit cycle generation," *IEEE American Control Conference*, 1990, Vol. 2, pp. 1198–1203.

9. W. Townsend and J. K. Salisbury, "The effect of Coulomb friction and stiction on force control," *IEEE International Conference on Robotics and Automation*, 1987, Vol. 2, pp. 883–889.
10. S. C. Southward, C. J. Radcliffe, and C. R. MacClure, "Robust nonlinear stick-slip friction compensation," *Journal of Dynamic Systems, Measurement, and Control*, **113,** 639–645, 1991.
11. D. Karnopp, "Computer simulation of stick-slip friction in mechanical dynamic system," *Journal of Dynamic Systems, Measurement, and Control*, **107,** 100–103, 1985.
12. C. Canudas, K. J. Astrom, and K. Braun, "Adaptive friction compensation in DC-motor drives," *IEEE Journal of Robotics and Automation*, **RA-3**(6), 681–685, 1987.
13. S. Yang and M. Tomizuka, "Adaptive pulse width control for precise positioning under the influence of stiction and Coulomb friction," *Journal of Dynamic Systems, Measurement, and Control*, **110,** 221–227, 1988.
14. J. W. Gilbart and G. C. Winston, "Adaptive compensation for an optical tracking telescope," *Automatica*, **10,** 125–131, 1974.
15. C. D. Walrath, "Adaptive bearing friction compensation based on recent knowledge of dynamic friction," *Automatica*, **20**(6), 717–727, 1984.
16. C. Canudas de Wit and V. Loand Seront, "Robust adaptive friction compensation," *IEEE International Conference on Robotics and Automation*, 1990, pp. 1383–1388.
17. J. Sampson and F. Morgan, et al. "Friction behavior during the slip portion of the stick-slip process," *Journal of Applied Physics*, **14,** 1943.
18. A. Tustin, "The effects of backlash and of speed-dependent friction on the stability of closed-cycle control system," *Journal of the Institute of Electrical Engineers*, **94**(2A), 143–151, 1947.
19. J. Y. S. Luh, M. W. Walker, and R. P. Paul, "Resolved-acceleration control of mechanical manipulators," *IEEE Trans. Autom. Contr.*, **AC-25**(3), 468–474, 1980.
20. A. Isidori, *Nonlinear Control System*, Springer-Verlag, New York, 1989.
21. J.-J. E. Slotine and W. Li, "On the adaptive control of robot manipulators," *International Journal of Robotics Research*, **6**(3), 49–59, 1987.
22. M. W. Spong and M. Vidysagar, *Robot Dynamics and Control*, Wiley, New York, 1989.
23. L. Cai and A. Abdalla, "Smooth robust tracking controller for uncertain robot manipulators," *IEEE International Conference on Robotics and Automation*, Atlanta GA, 1993, pp. 83–88.
24. Y. H. Chen, "On the deterministic performance of uncertain dynamic systems," *Inter. Journal Contr.*, **43**(5), 1557–1579, 1986.